Theoretical studies on structural and spectroscopic properties of photoelectrochemical cell ruthenium sensitizers, derivatives of AR20

ARTICLE *in* INTERNATIONAL JOURNAL OF QUANTUM CHEMISTRY · APRIL 2013

Impact Factor: 1.43 · DOI: 10.1002/qua.24009

5 AUTHORS, INCLUDING:

Jian Wang
Jilin University
66 PUBLICATIONS **188** CITATIONS
SEE PROFILE

Fu-Quan Bai
Jilin University
124 PUBLICATIONS **435** CITATIONS
SEE PROFILE

Theoretical Studies on Structural and Spectroscopic Properties of Photoelectrochemical Cell Ruthenium Sensitizers, Derivatives of AR20

Jie Chen,[a] Jian Wang,[a] Fu-Quan Bai,[a] Qing-Jiang Pan,[b] and Hong-Xing Zhang*[a]

Special efforts were devoted to improve the absorption behavior of AR20 in visible region. Density functional theory (DFT)-based approaches were applied to explore the electronic structure properties of AR20 and its derivatives. Time-dependent DFT results indicate that the ancillary ligand controls the molecular orbital (MO) energy levels and masters the absorption transition nature. The deprotonation of anchoring ligand not only affects the frontier MO energy levels but also determines the energy gaps of highest occupied MO–lowest unoccupied MO (LUMO) and LUMO–LUMO+1. Introducing thiophene groups into ancillary ligands would enhance the efficiency of the final dye-sensitized solar cell (DSSC). The absorption intensity of the thiophene substituted derivatives of AR20 is irrelevant with environment circumstance change, such as pH value. This special nature prognosticates the thiophene-substituted derivatives of AR20 which would have a broad application in DSSC. © 2012 Wiley Periodicals, Inc.

DOI: 10.1002/qua.24009

Introduction

With the consideration of the environmental safety and renewable issue, more and more attentions are paid to the usage of solar energy. As the dye-sensitized solar cells (DSSCs) own significant nature such as low cost and high efficiency of conversion of sunlight into electricity,[1–4] the attention to the DSSCs has risen to a well altitude. Sensitizer molecules as seen as core in the DSSCs have been widely investigated and improved. As the dye sensitizer, the following qualities are of vital importance. First, the sensitizer molecules should exhibit broad range absorptions in visible light. Second, the excited-state energy level of the sensitizer should match the conduction band of the thin optical transparent semiconductor film such as TiO_2 particles. Third, the sensitizer must show high-thermal stability. Furthermore, the presence of terminal, for example, acidic carboxylic in the sensitizer usually affords stable anchoring of the sensitizer to the semiconductor surface, so as to ensure a high-electronic coupling between the dye and the semiconductor, which is required for efficient charge injection.

Although numerous sensitizers such as metal-free organic dyes[5–8] and nonruthenium metal dyes[9–12] have been used, the highest energy conversion efficiency (up to 11%) was only achieved using Ru dyes, such as **N3**, **N719**, and **N749**,[13–16] in standard global air mass 1.5 sunlight. Up to now, **N3** and closely related analogs are still hotspot.[17] Generally, the ligands of some sensitizers derived from **N3** can be divided into three species, which are anchoring, ancillary, and NCS ligands. The NCS ligands popularly afford hole for regenerative dyes,[18] whereas anchoring ligands such as carboxylic groups are necessary to connect to TiO_2 film and to dominate the charge injection, so the 4,4′-carboxylicacid-4′-2,2′-bipyridine is widely assembled for Ru dyes. However, embellishing both NCS ligands and anchoring ligand could not efficaciously modulate the absorption spectrum range and achieve the advanced capability of DSSCs. Many groups have abandoned the improvement of the NCS and anchoring ligands for DSSCs efficiency.

For enhancing the device efficiency, there is already a successful strategy to release COOH segment in one of the 4,4′-dicarboxy-2,2′-bipyridine (**dcbpy**) anchoring ligands and embellish with the conjugated framework in [Ru(dcbpyH$_2$)$_2$(NCS)$_2$] (**N3**),[13] and this coordination groups are called ancillary ligands. To obtain high-light-harvesting efficiency in a broad range of visible light, annulations have been adopted as modified groups in ancillary ligands regularly, series of sensitizers such as **K19**,[19] **C101**,[20] **C103**,[21] **T18**,[22] and **CYC-B6S/L**[23] have been prepared. Noticeably, thiophene and its derivatives are adopted in the ancillary ligand frequently. When thiophene links to bipyridine, the efficiency of the DSSC is enhanced significantly. The reason is possibly that the modified groups reduce the system energy and the gap between

[a] J. Chen, J. Wang, F.-Q. Bai, H.-X. Zhang
State Key Laboratory of Theoretical and Computational Chemistry, Institute of Theoretical Chemistry, Jilin University, Changchun, 130023, People's Republic of China
Fax: (+86) 431 8894 5942
E-mail: zhanghx@mail.jlu.edu.cn

[b] Q.-J. Pan
Key Laboratory of Functional Inorganic Material Chemistry of Education Ministry, School of Chemistry & Materials Science, Heilongjiang University, Harbin 150080, People's Republic of China.

Contract grant sponsor: Natural Science Foundation of China; contract grant number: 20703015, 20973076, and 21003057.
Contract grant sponsor: Heilongjiang Provincial University of China (Program for New Century Excellent Talents); contract grant number: 1154-NCET-010.

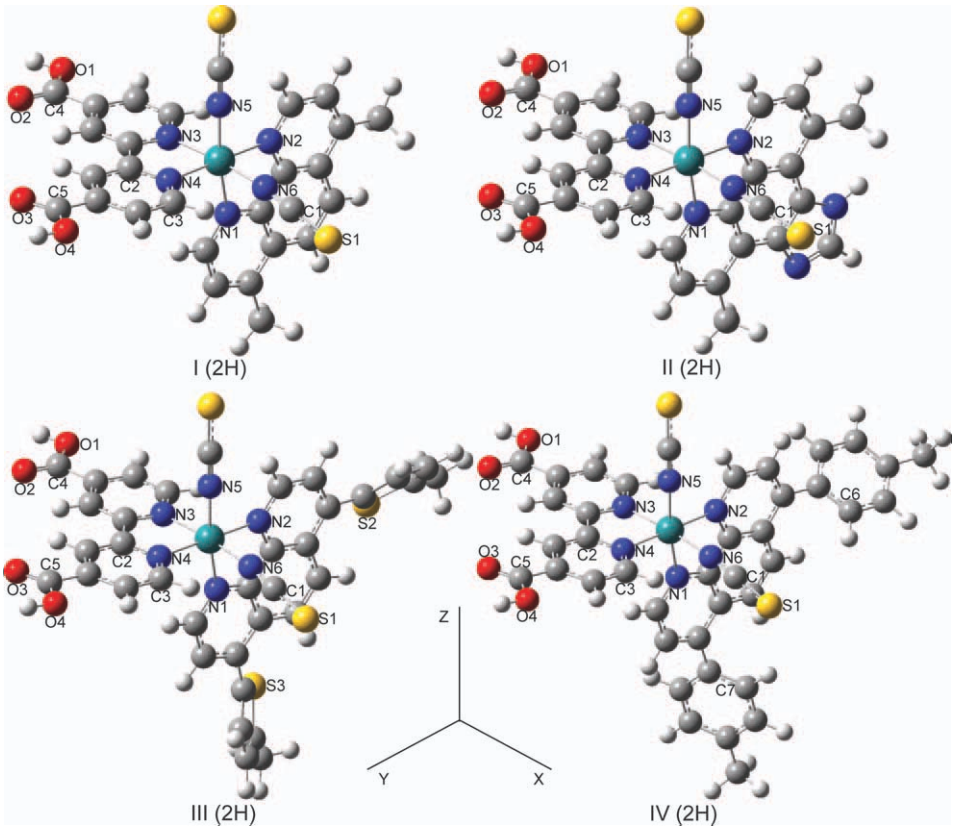

Figure 1. Optimized geometry structures of **I**, **II**, **III**, and **IV** in the ground state by TD-B3LYP (6-31G*). [Color figure can be viewed in the online issue, which is available at wileyonlinelibrary.com.]

highest occupied molecular orbital (HOMO) and lowest unoccupied molecular orbital (LUMO), resulting in more ample absorptions in visible range. In other words, our purpose is to find out the ancillary ligand with conjugated properties, whose orbital energy is lower than **dcbpy** and some of its derivatives.

In fact, in view of choice of ancillary ligand, there are some ligands with more aromatic properties than **dcbpy** such as 1,10-phenanthroline (**phen**), which can also form stabilized coordination bond with Ru center,[24–26] known as **AR20**. As the conjugation of ancillary ligands is reinforced, the whole absorption properties could be modified and the efficient DSSCs with rich absorptions in a broad range of visible light can be expected.

The detrimental effect is vital for further improvement of ancillary ligands. Concretely, resonance donating groups lead to the positive shift of Fermi level, which decreases the gap between the redox couple iodide/triiodide and Fermi level, resulting in a lower open-circuit potential.[27] Conversely, electron-withdrawing groups bring about a little negative shit to Fermi level, however, lower the short circuit current[28] significantly, that would also be against to the efficiency for DSSC devices. Therefore, we attempt to use the conjugation ligands for absorption improvement. Essentially, there is two tactics for increasing the conjugation of ancillary ligand. One is directly connecting the conjugated group on the ancillary ligand, such as thiophene and benzene. The other one is to expand the conjugated plane for electron localization, for example, 1*H*imidazo[4,5-f][1,10]phenanthroline. We designed some dye molecules:

[Ru (4,7-bismethyl-phen) ($dcbpyH_2$) $(NCS)_2$], [Ru (4,8-bismethyl-1*H*imidazo[4,5-f]phen) ($dcbpyH_2$) $(NCS)_2$], [Ru (4,7-bis (5-methylthiophen-2-yl)-phen) ($dcbpyH_2$) $(NCS)_2$], and [Ru (4,7-bis (5-methylbenzene-2-yl)-phen ($dcbpyH_2$) $(NCS)_2$], which are labeled as **I**, **II**, **III**, and **IV**, respectively, shown in Figure 1, among which only **I** has been synthesized in experiment at present.

We start our research to explore the effect of ancillary ligand choice, which influences energy levels and absorptions of Ru dyes. The dissolvent environments are necessary in theoretical calculations, so acetonitrile (ACN) has been used as solvent condition, which is applied in real DSSCs device. The degree of deprotonation decides the exact adsorbtion pattern for dyes to TiO_2 film.[29] Furthermore, varying the degree of protonation or deprotonation of the sensitizer, changes its electronic structure. Therefore, it is important to investigate how the energy and composition of the excited states could change as a function of the protonation of the terminal carboxylic groups. Overall, there should be an optimal degree of protonation of the sensitizer, in this condition, the power conversion efficiency of the cell could maximize[30] and the performance of DSSCs is better. In this work, it is investigated that the effect of different degrees of deprotonation (**2H**–**0H**) influences energy levels and spectrum absorptions in these systems, and we find the reasonable degrees of deprotonation selection about the particular dye molecule for better DSSC efficiency, that is key to electrons injection to TiO_2.[31] Then, it should be tested that the gap between LUMO and LUMO+1 is small, the cell will be efficient.[32] The aims of our theoretical calculations would provide support for experiment, such as the estimate for the efficiency of DSSCs and the proper conditions in practical application.

Computational Details and Theory

The geometries of dyes are dissymmetrical, so C_1 symmetry is adopted to settle the conformation of each one in both ground and excited states from 2H to 0H. The structures of ground state are fully optimized using density functional theory (DFT) with the B3LYP functional (Becke's three parameter functional and the Lee-Yang-Parr functional),[33] and the structures of excited state are fully optimized by unrestricted

B3LYP approach. On the basis of such calculations, spectroscopic properties related to absorption and emission are obtained using time-dependent DFT (TDDFT)[34] method. The polarizable continuum model (PCM)[35] is used to account for the solvent effects of ACN solvent molecules in optimization, absorption, and emission calculation.

It should be noted that there is a distinction between equilibrium and nonequilibrium calculation of transition energies in solution. In the Gaussian09, the equilibrium TDDFT calculation is achieved via a "state-specific type" correction to the default nonequilibrium TDDFT calculation using a solvent reaction field calculated in terms of the relaxed density of each electronic state. Such a density is obtained through the analytical gradient calculations.[36,37] Therefore, we selected the so-called nonequilibrium TDDFT calculation for singlet–singlet vertical excitations, which has been specifically designed for the study of absorption process. Meanwhile, we performed the equilibrium procedure for triplet TDDFT calculation to evaluate the singlet–triplet emission maximum.

In the recent years, TDDFT methods have been successfully used to calculate the singlet–singlet and singlet–triplet transitions.[38] Therefore, on the basis of optimized structures for ground state and excited state at DFT level of theory and the TDDFT method was used to calculate the absorption and emission transitions, respectively.

In the calculations, quasi-relativistic pseudopotential of Ru atom proposed by Hay and Wadt[39] with 16 valence electrons was used, and the LanL2DZ basis sets associated with the pseudopotential were adopted. Here, the basis sets were taken as Ru (8s7p6d/6s5p3d), S (16s10p1d/4s3p1d), N (10s4p1d/3s2p1d), and H (4s/2s). Thus, 630–626 basis functions and 310 electrons for **I** (**2H**–**0H**), 672–688 basis functions and 330 electrons for **II** (**2H**–**0H**), 786–782 basis functions and 394 electrons for **III** (**2H**–**0H**), and 814–810 basis functions and 390 electrons for **IV** (**2H**–**0H**) were included in the calculation. All calculations were accomplished using the Gaussian09 (Revision A.02) program package.[40]

Results and Discussion

Structures of I, II, III, and IV (2H–0H) in ground-states and excited-state structures

The full DFT optimizations on the four complexes (**2H**–**0H**) indicate that all the complexes have a $^1A_1$ symmetry ground state. Their structures are depicted in Figure 1, and the optimized main geometry parameters are listed in Table 1. As shown in Figure 1, the 12 complexes show a pseudooctahedral coordination for the Ru6N core because the Ru (II) atom adopts the low-spin $4d^6 5s^0$ electronic configuration. The coordination axis is shown in Figure 1. Anchoring ligand and one of the NCS ligands are nearly coplanar, so anchoring ligand-Ru—$N_6C_1S_1$ moiety lies on the *xy* plane, and the other NCS ligand is slightly tilted to the *z* axis.

In a simple Dewar, Chatt, and Duncanson model,[41] the bond interaction can be described as a donation from a σ MO of the ligand (i.e., CN^- or NCS^-) toward an empty d orbital of metal and a concurrent back-donation from a filled (or partially filled) d orbital to a π^* antibonding orbital of the ligand. The two processes can promote and strengthen each other. Because of the polypyridine ligands have σ-donating orbitals localized on N atom. π-donating or π^*-accepting orbitals delocalized on aromatic rings, back-donation between Ru and the π^* orbitals is

Table 1. Partial optimized geometry structural parameters of I, II, III, and IV in the ground state by TD-B3LYP (6–31G*), respectively. (S2 and S3 means dihedral angle between different thiophene plane and bipyridyl.).

	I			II			III			IV		
Parameters	2H	1H	0H	2H	1H	0H	2H	1H	0H	2H	1H	0H
Bond lengths (Å)												
Ru—N1	2.109	2.091	2.075	2.103	2.088	2.074	2.101	2.081	2.063	2.105	2.085	2.065
Ru—N2	2.104	2.096	2.093	2.096	2.086	2.082	2.096	2.085	2.083	2.099	2.090	2.088
Ru—N3	2.073	2.101	2.098	2.072	2.101	2.097	2.073	2.104	2.099	2.072	2.103	2.099
Ru—N4	2.069	2.072	2.096	2.070	2.074	2.098	2.073	2.077	2.099	2.071	2.074	2.097
Ru—N5	2.056	2.065	2.078	2.061	2.069	2.082	2.058	2.065	2.077	2.057	2.065	2.078
Ru—N6	2.068	2.090	2.102	2.068	2.089	2.103	2.066	2.087	2.097	2.069	2.088	2.101
N6—C1	1.185	1.182	1.180	1.185	1.182	1.180	1.185	1.182	1.181	1.185	1.182	1.181
C1—S1	1.631	1.640	1.647	1.631	1.640	1.647	1.631	1.640	1.645	1.631	1.640	1.646
N4—C2	1.364	1.365	1.366	1.364	1.364	1.365	1.364	1.364	1.365	1.364	1.364	1.365
N4—C3	1.347	1.348	1.347	1.347	1.348	1.347	1.347	1.348	1.347	1.347	1.348	1.347
C5—O3	1.213	1.214	1.253	1.213	1.214	1.253	1.213	1.214	1.252	1.214	1.214	1.253
C5—O4	1.351	1.358	1.255	1.351	1.358	1.255	1.351	1.358	1.255	1.351	1.358	1.255
C4—O2	1.214	1.253	1.252	1.214	1.253	1.252	1.214	1.253	1.252	1.214	1.253	1.252
C4—O1	1.353	1.251	1.256	1.353	1.251	1.256	1.353	1.251	1.255	1.353	1.251	1.255
Bond angles (deg)												
N1—Ru—N2	78.43	78.71	79.06	78.02	78.25	78.57	78.26	78.59	78.97	78.37	78.63	79.04
N3—Ru—N4	78.73	78.34	77.74	78.69	78.27	77.69	78.71	78.27	77.71	78.67	78.28	77.71
N5—Ru—N6	93.05	92.24	91.85	92.72	91.98	91.64	92.82	91.93	91.40	93.03	92.16	91.83
A dihedral angle(deg)												
S3/C7							47.87	48.89	48.76	52.68	53.29	52.63
S2/C6							47.07	49.24	49.87	52.38	52.76	52.90

significant.[42] Although we did not obtain the experimental values, however, we found the correlative data of their parent complexes, N3. The distance of Ru—N in bipyridine is around 2.036–2.058 Å; Ru—N in NCS is around 2.048–2.046 Å; N—C in NCS ligand is around 1.162–1.103 Å, and C—S in NCS is around 1.615–1.685 Å.[18] The differences between the experimental values and calculation data are in a permissible error, so we deem that the data from calculation is credible and reliable. In all the complexes, the calculated Ru—N1, two bond lengths become gradually shortened, whereas Ru—N3, 4, 5, 6 become elongated as the increase of the degree of deprotonation. The reason is that the decreased π back-donation from the metal Ru to the anchoring ligand π^* orbitals associated with the energy raise of the anchoring ligand-based unoccupied MOs and NCS ligand-based occupied MOs, which is opposite to ancillary ligand-based unoccupied MOs (see below).

It is noticed that the bond length of Ru—N5 is shorter than the Ru—N6 by about 0.01–0.03 Å, probably as a result that the NCS ligand in *xy* plane is trans to the stronger electron-attracting anchoring ligand compared to the ancillary ligand, which are less attracting.

In this research, the UB3LYP method is used to optimize the structures of **III** in excited state. The main geometry parameters of the complexes in triplet excited state are presented in Supporting Information, Table S1. In the lowest energy excited states, the Ru—N band distances show a similar variation trend, that Ru—N1, 2 are longer by about 0.01–0.03 Å, Ru—N5, 6 are shorter by 0.03–0.06 Å than those in ground state. The variation of the bond lengths indicate that the electrons are promoted from Ru atom and NCS ligands to ancillary ligands and the interaction between the Ru atom and ancillary ligands is weakened on excitation. This evidence suggests that a ^{3}MLCT (metal to ligand charge transfer)/^{3}ligand to ligand charge transfer (LLCT) transition should be responsible for the lowest energy emission. Interestingly, in the excited state about **III** (**0H**), one of the dihedral angle between thiophene (S_3) and bipyridine become nearly complanate, that would significantly decrease the energy levels distributing on the ancillary ligand, and perhaps, the reason that the thiophene is frequently adopted in dyes molecules.

Absorption spectra

Electronic structures It would be useful to examine the nature of the frontier MOs for these Ru (II) complexes to provide the framework for excited-state TDDFT in the subsequent section. Moreover, the frontier MOs play a relevant role in such systems, because they rule the electronic excitations and transition character. The frontier MOs are plotted according to the corresponding energies in Figure 2 for complexes **I**, **II**, **III**, and **IV** (**2H**–**0H**), to illuminate the effect of the deprotonation. The frontier MO compositions of **I** (**2H**–**0H**) in ACN are compiled in Table 2, and others are shown in Supporting Information,

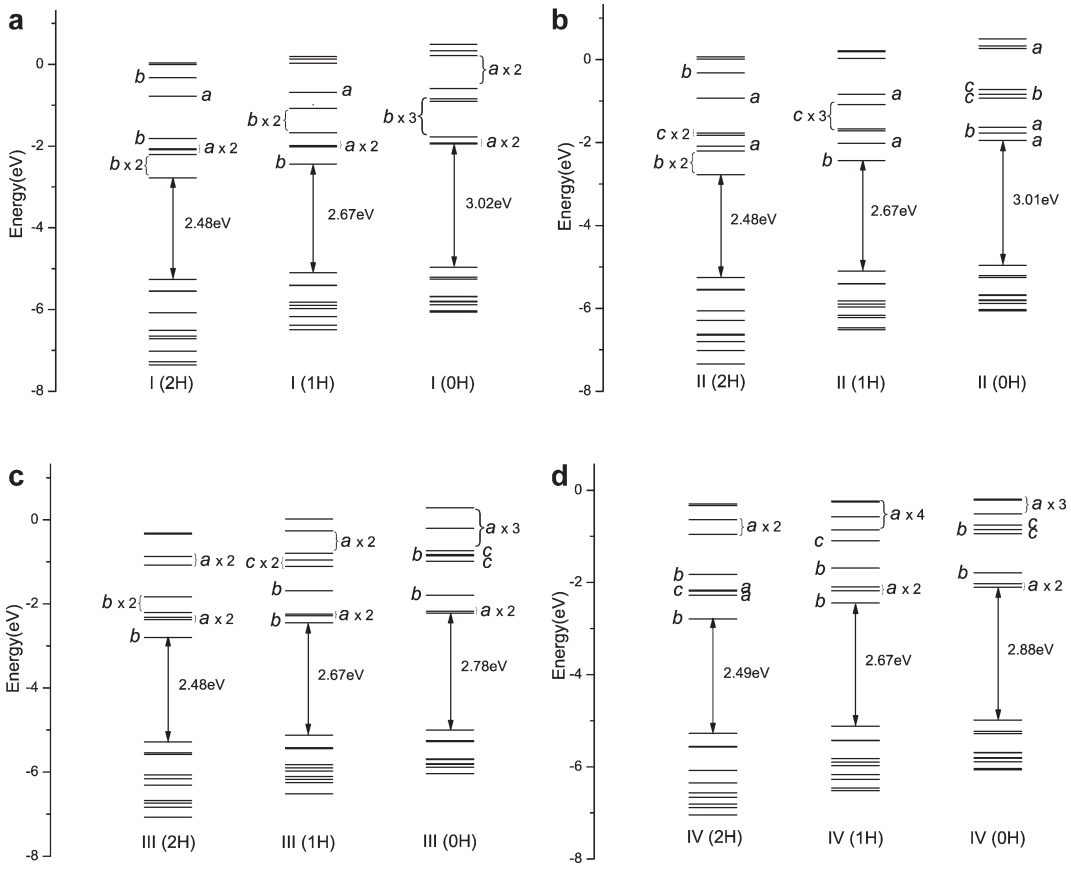

Figure 2. Plot of the frontier MOs relevant to the absorptions for **I**, **II**, **III**, and **IV** in ACN solution, calculated by TD-B3LYP (6-31G*). (Especially, *a* type means π or π^* orbital of ancillary ligands; *b*: orbital of anchoring ligands; *c*: mixed *a* and *b*.).

Table 2. Partial MO compositions (%) of II (2H) (a), II (1H) (b) and II (0H) (c) in ACN by TD-B3LYP (6–31G*).

		Composition (%)						
MO	Energy (eV)	Ru	Anch	COOH	COO^-	Anci	NCS	Assignment of orbital
(a) **I (2H)**								
LUMO+8	0.0351	27.0	19.2	0.7		39.0	14.1	$d_{x^2-y^2}$(Ru)–π*(NCS) π*(anci)
LUMO+7	−0.0049	36.0	6.6	0.1		38.0	19.2	$d_{x^2-y^2}$(Ru)–π*(NCS) π*(anci)
LUMO+6	−0.3282	0.3	88.4	9.1		1.8	0.4	π*(anch)
LUMO+5	−0.7821	4.0	1.7	0.4		92.8	1.2	π*(anci)
LUMO+4	−1.8139	1.4	88.3	8.0		1.9	0.4	π*(anch)
LUMO+3	−2.0681	5.3	3.5	1.1		89.2	0.8	π*(anci)
LUMO+2	−2.0931	1.3	2.4	0.5		95.6	0.2	π*(anci)
LUMO+1	−2.2050	1.7	65.2	26.8		6.1	0.2	π*(anch)–p_x(COOH)
LUMO+0	−2.7821	9.0	74.9	12.9		1.6	1.6	π*(anch)
HOMO–LUMO energy gap								
HOMO−0	−5.2635	49.5	4.1	0.4		3.6	42.3	d_{xz}(Ru)–π*(NCS)
HOMO−1	−5.5495	47.6	4.0	0.0		5.2	43.2	d_{yz}(Ru)– π*(NCS)
HOMO−2	−5.5574	44.0	5.5	0.6		3.3	46.6	d_{xy}(Ru)– π*(NCS)
HOMO−3	−6.0755	0.8	0.4	–		0.8	97.9	π*(NCS)
HOMO−4	−6.5082	24.7	2.8	0.1		28.0	44.4	d_{yz}(Ru)–π*(NCS) π*(anci)
HOMO−5	−6.6521	38.1	6.5	0.5		4.2	50.6	d_{xy}(Ru)–π*(NCS)
HOMO−6	−6.7161	29.6	5.3	0.5		15.9	48.7	d_{xz}(Ru)–π*(NCS) π*(anci)
HOMO−7	−7.0187	23.7	4.1	0.2		57.4	14.6	d_{yz}(Ru)–π*(NCS) π (anci)
HOMO−8	−7.2764	3.6	7.6	0.1		86.6	2.1	π (anci)
HOMO−9	−7.3561	2.3	89.7	0.6		6.2	1.2	π (anch)
(b) **I (1H)**								
LUMO+8	0.1918	44.7	23.2	0.2	0.2	8.2	23.5	d_{x_2-y2}(Ru)–π*(NCS) π*(anch)
LUMO+7	0.1320	3.3	2.4	0.1	–	93.3	0.8	π*(anci)
LUMO+6	0.0288	1.3	82.9	13.3	0.4	1.7	0.5	π*(anch)–p_x(COOH)
LUMO+5	−0.6874	4.5	4.7	–	0.3	89.6	1.0	π*(anci)
LUMO+4	−1.0776	3.5	83.3	0.6	5.8	5.7	1.1	π*(anch)
LUMO+3	−1.6792	1.0	86.5	10.1	1.2	0.9	0.3	π*(anch)
LUMO+2	−1.9889	4.9	1.2	–	–	93.1	0.8	π*(anci)
LUMO+1	−2.0210	1.5	0.6	–	–	97.5	0.3	π*(anci)
LUMO+0	−2.4376	7.4	74.0	15.5	0.4	1.6	1.1	π*(anch)–p_x(COOH)
HOMO–LUMO energy gap								
HOMO−0	−5.1027	53.7	3.7	–	0.2	4.0	38.3	d_{xz}(Ru)–π*(NCS)
HOMO−1	−5.4053	49.9	5.4	0.5	0.1	3.9	40.2	d_{xy}(Ru)–π*(NCS)
HOMO−2	−5.4143	50.4	4.0	0.1	0.3	5.6	39.6	d_{yz}(Ru)–π*(NCS)
HOMO−3	−5.8225	–	15.3	–	84.4	–	0.2	p_y/p_z(COO^-)
HOMO−4	−5.8970	–	40.0	–	59.8	–	0.1	p_z(COO^-) p_z(anch)
HOMO−5	−5.9729	0.6	0.4	–	0.0	0.7	98.3	π*(NCS)
HOMO−6	−6.1689	–	2.0	–	97.8	–	0.2	p_x(COO^-)
HOMO−7	−6.3814	24.7	2.6	–	0.1	21.0	51.6	d_{yz}(Ru)–π*(NCS) π(anci)
HOMO−8	−6.4913	32.9	7.1	0.5	0.3	4.1	55.1	d_{xy}(Ru)–π*(NCS)
HOMO−9	−6.5651	26.3	5.6	0.1	0.4	11.4	56.3	d_{xz}(Ru)–π*(NCS)
(c) **I (0H)**								
LUMO+8	0.4871	42.7	14.3		0.1	30.7	12.2	$d_{x^2-y^2}$(Ru)–π*(NCS) π*(anci)
LUMO+7	0.3312	44.3	22.7		0.2	7.8	25.0	$d_{x^2-y^2}$(Ru)–π*(NCS) π*(anch)
LUMO+6	0.2131	1.6	1.8		–	96.3	0.4	π*(anci)
LUMO+5	−0.5894	4.6	9.6		0.5	84.3	1.0	π*(anci)
LUMO+4	−0.8457	1.8	87.5		9.3	0.9	0.5	π*(anch)
LUMO+3	−0.9081	3.9	79.3		3.3	12.8	0.7	π*(anch)
LUMO+2	−1.7701	6.6	79.3		3.1	9.6	1.4	π*(anch)
LUMO+1	−1.9244	4.8	8.5		0.3	85.5	1.0	π*(anci)
LUMO+0	−1.9464	1.3	1.2		0.0	97.2	0.2	π*(anci)
HOMO – LUMO Energy Gap								
HOMO−0	−4.9675	56.4	3.8		0.2	5.0	34.6	d_{xz}(Ru)–π*(NCS)
HOMO−1	−5.2102	55.8	5.8		0.4	4.6	33.4	d_{xy}(Ru)–π*(NCS)
HOMO−2	−5.2578	55.9	4.1		0.5	6.2	33.3	d_{yz}(Ru)–π*(NCS)
HOMO−3	−5.6793	–	15.4		84.3	–	0.3	p_y(COO^-)
HOMO−4	−5.6921	0.1	14.8		84.8	–	0.3	p_z(COO^-)
HOMO−5	−5.8004	0.1	39.7		59.8	–	0.4	p_y/p_z(COO^-) p_y/p_z(anch)
HOMO−6	−5.8162	0.1	39.9		60.0	0.1	0.0	p_y/p_z(COO^-) p_y/p_z(anch)
HOMO−7	−5.8837	0.5	0.4		0.1	0.6	98.4	π*(NCS)
HOMO−8	−6.0323	–	4.6		95.2	–	0.2	p_x(COO^-)
HOMO−9	−6.0619	–	0.8		99.0	–	0.1	p_x(COO^-)

Table S2. The electron density diagrams of main frontier MOs for **II** (2H) and **III** (2H) in ACN are shown in Figure 3 to give out a clear illustration of improvement effect.

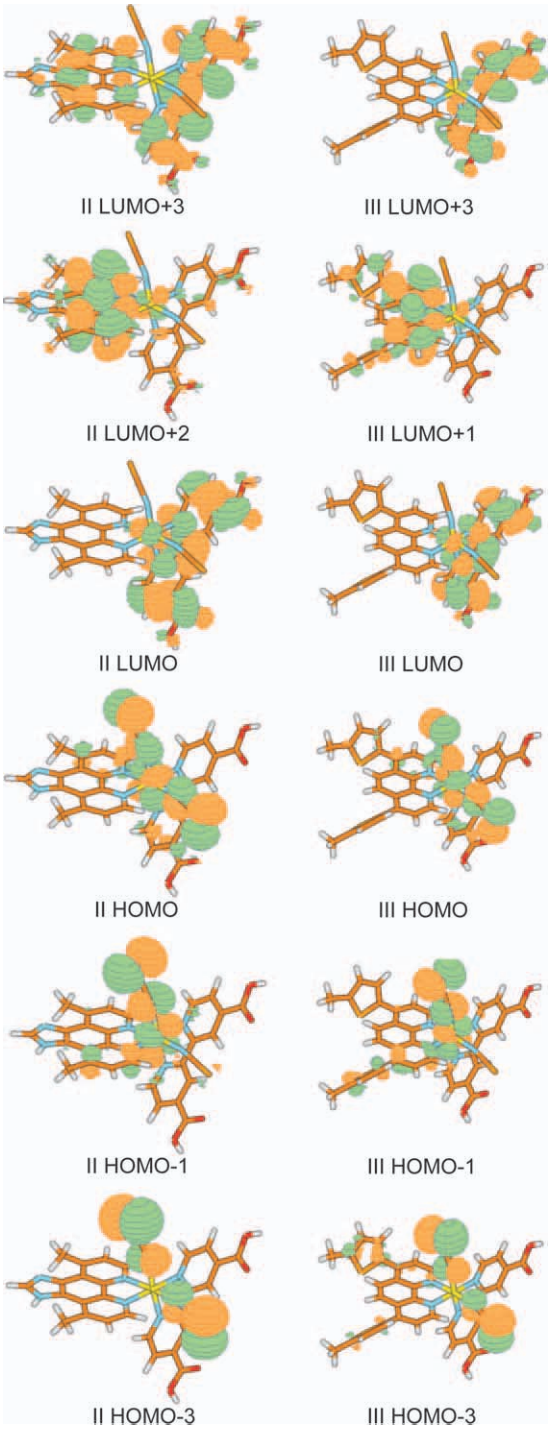

Figure 3. Electron density diagrams of the frontier MOs relevant to the absorptions of **II** (**2H**) and **III** (**2H**) in ACN by TD-B3LYP (6-31G*). [Color figure can be viewed in the online issue, which is available at wileyonline library.com.]

For all the considered complexes, the pattern of the occupied MOs and unoccupied MOs are qualitatively similar. As depicted in Figure 2, the unoccupied MOs orbitals can be classified as three types, which are labeled as *a*, *b,* and *c*, respectively. The *a* type is that the contribution comes from the π or π^* orbit of ancillary ligand, The *b* type is primary from anchoring ligand, and the *c* type is mixed contribution from both ancillary and anchoring ligands above. The deprotonation effect mostly alters the distribution of unoccupied MOs. As the increasing degree of deprotonation, there is more contribution from ancillary ligand toward the low-energy unoccupied MOs.

Let us focus on LUMO, LUMO+1, LUMO+2, and LUMO+3 orbitals, which decide the absorptions in visible range. In **I** system, LUMO+3, LUMO+2; LUMO+2, LUMO+1; and LUMO+1, LUMO are obtained, respectively, that localized on the ancillary ligand from **2H** to **0H**. Compared to **I**, it is the similar case in **II** system, there is merely unique *c* type MOs, that electron delocalized on both anchoring and ancillary ligand for some orbitals. In a sense, the contribution to unoccupied MOs from ancillary ligands has increased in **II** system.

When the thiophene or benzene is directly introduced to ancillary ligand in following systems, the composition of the LUMOs contains more contribution from ancillary ligand, even that all LUMO, LUMO+1, and LUMO+3 in **III** (**0H**) meet the condition. In **III** and **IV** systems, it could be concluded that contribution of thiophene is not neglectable, but benzene: **III** system owns two lowest energy unoccupied MOs with close energy about 0.05 eV, which ensures the more widely absorptions than others in visible light. Finally, we get sufficiently close energy between LUMO and LUMO+1 in **I** (**0H**) and **III** (**0H**), whose gap is 0.0220 and 0.0427 eV, respectively. However, the close-lying LUMO and LUMO+1 do not show up in the species with lower degree of deprotonation.

Similarly, the occupied MOs can be classified as four types, respectively. The first type has essentially ruthenium d character with a sizable contribution from the NCS ligand orbitals, mixed in an antibonding fashion with the metal atom. The second type is one kind of NCS π^* orbitals, that may contain some contribution from the ancillary ligand. The significant thiocyanate character in HOMOs has been already found in the N3 dye[43,44] and seems to play an important role in the regeneration of DSSCs.[18] The third type is mainly localized on the COO^- ligands with a little anchoring ligand component. The last type is composed of π^* banding orbitals and localizes on the ancillary ligands, which only exist in some **2H** systems. In all species, HOMO, HOMO−1, and HOMO−2 are antibonding combinations of the Ru d orbitals with the NCS π orbitals. Whereas in high degree of deprotonation, the third type of orbitals appeared in the high-energy occupied MOs. As the constituent of highest energy occupied MOs hardly change in each system, the absorptions would not be influenced obviously.

The MO energy levels of the various deprotonated complexes (**2H**–**0H**) in ACN solution show that deprotonation of the terminal COOH group results in less stabilization of the unoccupied orbitals which localize on the anchoring ligand moieties. For each step of deprotonation, the variation of the unoccupied orbitals is more dramatic with respect to the occupied orbitals. Thus, the HOMO to LUMO energy gaps increase from 2.48 to 3.02 eV (**I**: the HOMO to LUMO energy gap of **2H**, **1H**, and **0H** are 2.48, 2.67, and 3.02 eV, respectively, see Fig. 2.). All other systems follow this tendency. The

Table 3. Calculated absorptions (λ > 400nm) of II (2H–0H) in ACN by TD-B3LYP (6–31G*) (CI: configuration interaction; anch: anchoring ligands; anci: ancillary ligand; thi: thiophene).

	Peak	Enm (eV)	Oscillator strength	Config (CI coeff)	Assignment
I (2H)	1	703.4 (1.76)	0.0214	H−0 → L+0 (0.68)	d_{xz} (Ru)–π* (NCS) → π* (anch)
	2	564.7 (2.20)	0.0707	H−2 → L+0 (0.65)	d_{xy} (Ru)–π* (NCS) → π* (anch)
	3	504.6 (2.46)	0.0364	H−0 → L+3 (0.57)	d_{xz} (Ru)–π* (NCS) → π* (anci)
				H−0 → L+1 (0.40)	d_{xz} (Ru)–π* (NCS) → π* (anch)–p_x (COOH)
		487.5 (2.54)	0.0631	H−0 → L+1 (0.49)	d_{xz} (Ru)–π* (NCS) → π* (anch)–p_x (COOH)
				H−0 → L+3 (0.37)	d_{xz} (Ru)–π* (NCS) → π* (anci)
				H−0 → L+2 (0.29)	d_{xz} (Ru)–π* (NCS) → π* (anci)
		480.9 (2.58)	0.0314	H−0 → L+2 (0.61)	d_{xz} (Ru)–π* (NCS) → π* (anci)
				H−0 → L+1 (0.22)	d_{xz} (Ru)–π* (NCS) → π* (anch)–p_x (COOH)
		453.8 (2.73)	0.0228	H−1 → L+1 (0.65)	d_{yz} (Ru)–π* (NCS) → π* (anch)–p_x (COOH)
	4	444.6 (2.79)	0.0494	H−2 → L+3 (0.39)	d_{xy} (Ru)–π* (NCS) → π* (anci)
				H−3 → L+1 (0.38)	π* (NCS) → π* (anch)–p_x (COOH)
				H−2 → L+1 (0.23)	d_{xy} (Ru)–π* (NCS) → π* (anch)–p_x (COOH)
				H−1 → L+3 (0.22)	d_{yz} (Ru)–π* (NCS) → π* (anci)
				H−1 → L+2 (0.21)	d_{yz} (Ru)–π* (NCS) → π* (anci)
		443.7 (2.79)	0.0232	H−3 → L+0 (0.53)	π* (NCS) → π (anch)
				H−2 → L+1 (0.33)	d_{xy} (Ru)–π* (NCS) → π* (anch)–p_x (COOH)
				H−2 → L+3 (0.23)	d_{xy} (Ru)–π* (NCS) → π* (anci)
		440.5 (2.81)	0.0336	H−1 → L+2 (0.53)	d_{yz} (Ru)–π* (NCS) → π* (anci)
				H−2 → L+1 (0.27)	d_{xy} (Ru)–π* (NCS) → π* (anch)–p_x (COOH)
				H−3 → L+0 (0.22)	π* (NCS) → π (anch)
		430.0 (2.88)	0.0456	H−1 → L+3 (0.55)	d_{yz} (Ru)–π* (NCS) → π* (anci)
				H−1 → L+2 (0.28)	d_{yz} (Ru)–π* (NCS) → π* (anci)
I (1H)	1	642.8 (1.93)	0.0052	H−0 → L+0 (0.68)	d_{xz} (Ru)–π* (NCS) → π* (anch)–p_x (COOH)
	2	524.0 (2.37)	0.0475	H−0 → L+2 (0.60)	d_{xz} (Ru)–π* (NCS) → π* (anci)
				H−1 → L+0 (0.25)	d_{xy} (Ru)–π* (NCS) → π* (anch)–p_x (COOH)
				H−0 → L+1 (0.21)	d_{xz} (Ru)–π* (NCS) → π* (anci)
		510.7 (2.43)	0.0781	H−1 → L+0 (0.49)	d_{xy} (Ru)–π* (NCS) → π* (anch)–p_x (COOH)
				H−0 → L+2 (0.34)	d_{xz} (Ru)–π* (NCS) → π* (anci)
				H−0 → L+1 (0.26)	d_{xz} (Ru)–π* (NCS) → π* (anci)
				H−2 → L+0 (0.23)	d_{yz} (Ru)–π* (NCS) → π* (anch)–p_x (COOH)
		497.3 (2.49)	0.0347	H−0 → L+1 (0.59)	d_{xz} (Ru)–π* (NCS) → π* (anci)
				H−1 → L+0 (0.27)	d_{xy} (Ru)–π* (NCS) → π* (anch)–p_x (COOH)
	3	452.7 (2.74)	0.0347	H−2 → L+1 (0.52)	d_{yz} (Ru)–π* (NCS) → π* (anci)
				H−1 → L+1 (0.30)	d_{xy} (Ru)–π* (NCS) → π* (anci)
				H−2 → L+2 (0.25)	d_{yz} (Ru)–π* (NCS) → π* (anci)
		443.4 (2.80)	0.0681	H−0 → L+3 (0.52)	d_{xz} (Ru)–π* (NCS) → π* (anch)
				H−2 → L+1 (0.33)	d_{yz} (Ru)–π* (NCS) → π* (anci)
				H−2 → L+2 (0.32)	d_{yz} (Ru)–π* (NCS) → π* (anci)
		435.4 (2.85)	0.0301	H−2 → L+2 (0.51)	d_{yz} (Ru)–π* (NCS) → π* (anci)
				H−0 → L+3 (0.40)	d_{xz} (Ru)–π* (NCS) → π* (anch)
I (0H)	1	539.6 (2.30)	0.0152	H−0 → L+1 (0.68)	d_{xz} (Ru)–π* (NCS) → π* (anci)
	2	464.9 (2.67)	0.0576	H−2 → L+1 (0.53)	d_{yz} (Ru)–π* (NCS) → π* (anci)
				H−2 → L+2 (0.33)	d_{yz} (Ru)–π* (NCS) → π* (anch)
		456.5 (2.72)	0.1004	H−1 → L+2 (0.45)	d_{xy} (Ru)–π* (NCS) → π* (anch)
				H−2 → L+0 (0.38)	d_{yz} (Ru)–π* (NCS) → π* (anci)
				H−2 → L+1 (0.29)	d_{yz} (Ru)–π* (NCS) → π* (anci)
				H−2 → L+2 (0.21)	d_{yz} (Ru)–π* (NCS) → π* (anch)
		433.8 (2.86)	0.0409	H−2 → L+2 (0.46)	d_{yz} (Ru)–π* (NCS) → π* (anch)
				H−1 → L+2 (0.40)	d_{xy} (Ru)–π* (NCS) → π* (anch)

deprotonated course could result in more negative charge concentrated on the carboxylic groups, which would increase the orbital energy of anchoring ligand. This similar effect has been found in **N3** and **N3**-derived dyes.[18,45,46]

Absorption spectra of I and II in ACN. The absorption spectra of **2H**–**0H** in the ACN solution were obtained using TDDFT (B3LYP) calculations with PCM. The calculated absorptions associated with the corresponding oscillator strengths, main configurations, and the assignments are summarized in Table 3 (Supporting Information, **II** in Table S3). The fitted Gaussian-type absorption curves with the calculated absorption data of **I** and **II** are shown in Figures 4 and 5.

We divide the absorption spectra into two parts; the 400 nm is regulated as boundary. When absorption wavelength (λ) is longer than 400 nm, it means that visible light could be used as solar power. In addition, the absorption spectra is excessively complicate to analyze when $\lambda < 400$ nm.

For **I** (**2H**), there are four absorption peaks when $\lambda >$ 400 nm. The lowest energy absorption in ACN is calculated at 703 nm. Due to the largest coefficient (about 0.68), the excitation H−0 → L+0 is responsible for the absorption. As shown

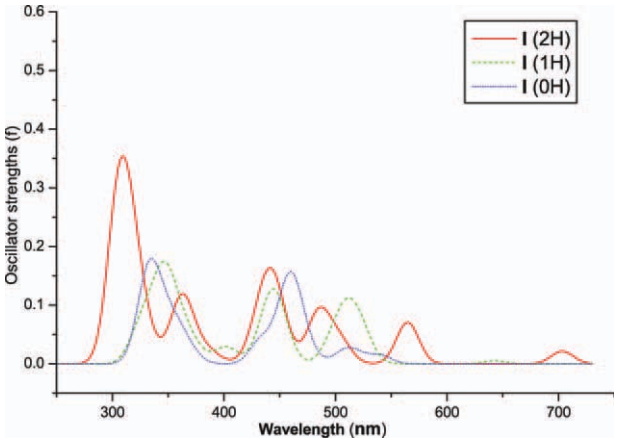

Figure 4. Simulated absorption spectra of **I** (**2H–0H**) in ACN by TD-B3LYP (6-31G*). [Color figure can be viewed in the online issue, which is available at wileyonlinelibrary.com.]

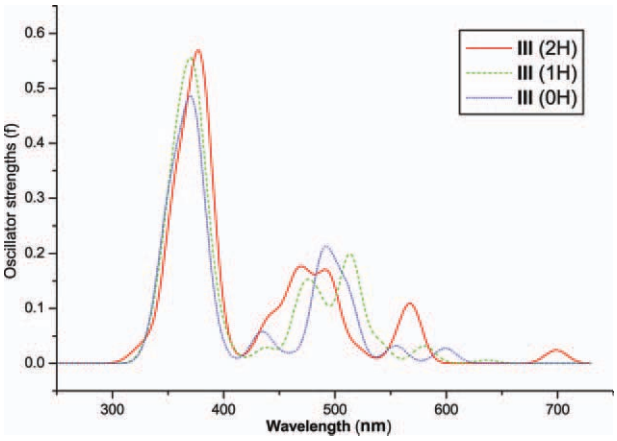

Figure 6. Simulated absorption spectra of **III** (**2H–0H**) in ACN by TD-B3LYP (6-31G*). [Color figure can be viewed in the online issue, which is available at wileyonlinelibrary.com.]

in Supporting Information, Table S2, HOMO is formed by 50% d_{xz}(Ru) and 42% NCS Π* orbitals, whereas the LUMO is delocalized over the π* orbitals of anchoring ligand. Therefore, the absorption spectra at 703 nm could be assigned as the combination of d_{xz} (Ru) $\rightarrow$ π* (anch) charge transfer (MLCT) and Π*(NCS) $\rightarrow$ π* (anch) (LLCT) transitions, where Π is shown that both of the NCS ligands take part in the conjugation with d orbitals of Ru. Here, anchoring ligand is signed as L_1, ancillary ligand as L_2, and NCS as L_3. The character of charge transition about the lowest energy absorption is marked as ML_1CT and L_3L_1CT, similarly, the other three peaks in this range are marked as $ML_{1\ or\ 2}CT$ and $L_3L_{1\ or\ 2}CT$. In this range, involved orbitals are from HOMO$-$3 to LUMO$+$3. Considering the oscillator strengths and coefficient in CI wave functions, the contribution of ancillary ligands to absorption increases as λ becomes shorter.

When $\lambda < 400$ nm, the absorption peaks are similar in **I** (**2H**, **1H**, **0H**). Both anchoring ligand and ancillary ligand contribute a lot to absorptions, and $ML_{1/2}CT$ and $L_3L_{1/2}CT$ are primary transitions, among them L_3L_2CT play a more important role in this range of absorption wavelength.

For **I** (**1H**) and **I** (**0H**), there is slight difference about absorption characters with respect to **I** (**2H**). First, the oscillator strength of the lowest absorption in **I** (**1H**) is very weak, and in **I** (**0H**) there is no ML_1CT transitions in lowest absorption. It is caused by the inductive effect of the substituent on the anchoring ligand. Then, the energy levels of the unoccupied anchoring ligand π* orbitals increase. Second, there are no significant absorptions when $\lambda > 550$ nm. Generally, when the degree of deprotonation increases, the extensive absorption will not appear in long-wavelength range, which would not benefit the efficiency of DSSC. In **I** system, the differences of absorption oscillator strength from **2H** to **0H** are not notable in 400–550 nm range, so the best dye molecule should be **I** (**2H**) in the whole visible range. The excited states of I (**1H**), which give birth of intense absorptions at 440 and 510 nm are principally referred to LUMO and LUMO$+$1, with the strong oscillator strength 0.0781 and 0.0.0681 in ACN. Compared with absorptions at 460 and 520 nm in experiment[24]

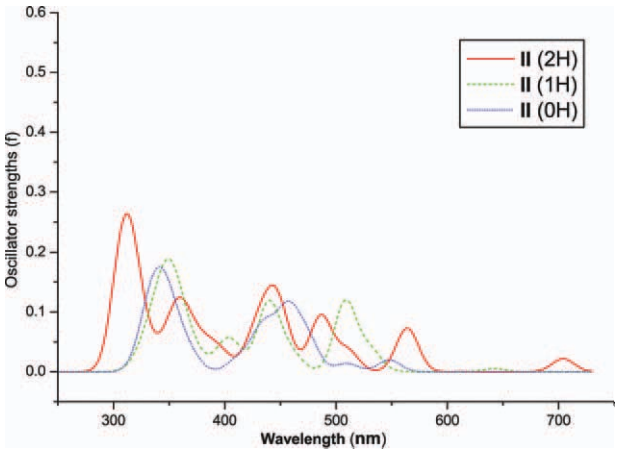

Figure 5. Simulated absorption spectra of **II** (**2H–0H**) in ACN by TD-B3LYP (6-31G*). [Color figure can be viewed in the online issue, which is available at wileyonlinelibrary.com.]

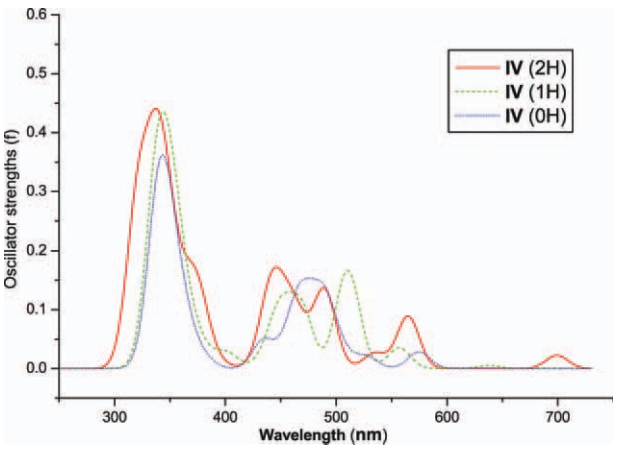

Figure 7. Simulated absorption spectra of **IV** (**2H–0H**) in ACN by TD-B3LYP (6-31G*). [Color figure can be viewed in the online issue, which is available at wileyonlinelibrary.com.]

Table 4. Calculated absorptions (λ > 400nm) of III (2H – 0H) in ACN by TD-B3LYP (6–31G*).

	Peak	Enm (eV)	Oscillator strength	Config (CI coeff)	Assignment
III (2H)	1	698.7 (1.77)	0.0241	H−0 → L+0(0.68)	d_{xz}(Ru)–π*(NCS) → π*(anch)–p_x(COOH)
	2	568.2 (2.18)	0.1027	H−2 → L+0 (0.60)	d_{xy}(Ru)–π*(NCS) → π*(anch)–p_x(COOH)
				H−0 → L+1(0.26)	d_{xz}(Ru)–π*(NCS) → π*(anci) π*(thi)
	3	519.0 (2.39)	0.0266	H−0 → L+2(0.66)	d_{xz}(Ru)–π*(NCS) → π*(anci) π*(thi)
				H−1 → L+1(0.20)	d_{yz}(Ru)–π*(NCS) → π*(anci) π*(thi)
		495.1 (2.50)	0.1310	H−1 → L+1(0.45)	d_{yz}(Ru)–π*(NCS) → π*(anci) π*(thi)
				H−0 → L+3(0.44)	d_{xz}(Ru)–π*(NCS) → π*(anch)–p_x(COOH)
				H−2 → L+1(0.25)	d_{xy}(Ru)–π*(NCS) → π*(anci) π*(thi)
		476.6 (2.60)	0.0777	H−1 → L+1(0.39)	d_{yz}(Ru)–π*(NCS) → π*(anci) π*(thi)
				H−1 → L+2(0.36)	d_{yz}(Ru)–π*(NCS) → π*(anci) π*(thi)
				H−0 → L+3(0.36)	d_{xz}(Ru)–π*(NCS) → π*(anch)–p_x(COOH)
		465.0 (2.67)	0.1130	H−1 → L+2(0.58)	d_{yz}(Ru)–π*(NCS) → π*(anci) π*(thi)
				H−1 → L+1(0.24)	d_{yz}(Ru)–π*(NCS) → π*(anci) π*(thi)
		446.3 (2.78)	0.0273	H−3 → L+0(0.62)	π*(NCS) → π*(anch)–p_x(COOH)
		441.6 (2.81)	0.0297	H−2 → L+3(0.63)	d_{xy}(Ru)–π*(NCS) → π*(anch)–p_x(COOH)
		436.0 (2.84)	0.0269	H−0 → L+4(0.68)	d_{xz}(Ru)–π*(NCS) → π*(anch)
III (1H)	1	636.3 (1.95)	0.0059	H−0 → L+0(0.69)	d_{xz}(Ru)–π*(NCS) → π*(anch)–p_x(COOH)
	2	579.9 (2.14)	0.0316	H−0 → L+1(0.63)	d_{xz}(Ru)–π*(NCS) → π*(anci) π*(thi)
				H−0 → L+2(0.27)	d_{xz}(Ru)–π*(NCS) → π*(anci) π*(thi)
	3	539.0(2.30)	0.0369	H−0 → L+2(0.63)	d_{xz}(Ru)–π*(NCS) → π*(anci) π*(thi)
				H−0 → L+1(0.22)	d_{xz}(Ru)–π*(NCS) → π*(anci) π*(thi)
		513.7 (2.41)	0.1890	H−2 → L+0(0.59)	d_{xy}(Ru)–π*(NCS) → π*(anch)–p_x(COOH)
				H−1 → L+1(0.34)	d_{yz}(Ru)–π*(NCS) → π*(anci) π*(thi)
		486.5 (2.55)	0.0888	H−1 → L+1(0.48)	d_{yz}(Ru)–π*(NCS) → π*(anci) π*(thi)
				H−1 → L+2(0.34)	d_{yz}(Ru)–π*(NCS) → π*(anci) π*(thi)
				H−2 → L+0(0.25)	d_{xy}(Ru)–π*(NCS) → π*(anch)–p_x(COOH)
		470.2 (2.64)	0.1070	H−1 → L+2(0.61)	d_{yz}(Ru)–π*(NCS) → π*(anci) π*(thi)
				H−1 → L+1(0.22)	d_{yz}(Ru)–π*(NCS) → π*(anci) π*(thi)
	4	437.9 (2.83)	0.0280	H−0 → L+3(0.68)	d_{xz}(Ru)–π*(NCS) → π*(anch)
III (0H)	1	599.0 (2.07)	0.0276	H−0 → L+0(0.62)	d_{xz}(Ru)–π*(NCS) → π*(anci) π*(thi)
				H−0 → L+1(0.28)	d_{xz}(Ru)–π*(NCS) → π*(anci) π*(thi)
	2	554.7 (2.24)	0.0317	H−0 → L+1(0.61)	d_{xz}(Ru)–π*(NCS) → π*(anci) π*(thi)
				H−2 → L+0(0.22)	d_{yz}(Ru)–π*(NCS) → π*(anci) π*(thi)
				H−0 → L+0(0.21)	d_{xz}(Ru)–π*(NCS) → π*(anci) π*(thi)
	3	512.3 (2.42)	0.0964	H−2 → L+0(0.47)	d_{yz}(Ru)–π*(NCS) → π*(anci) π*(thi)
				H−1 → L+1(0.37)	d_{xy}(Ru)–π*(NCS) → π*(anci) π*(thi)
				H−1 → L+0(0.20)	d_{xy}(Ru)–π*(NCS) → π*(anci) π*(thi)
		505.7 (2.45)	0.0239	H−0 → L+2(0.52)	d_{xz}(Ru)–π*(NCS) → π*(anch)
				H−1 → L+1(0.42)	d_{xy}(Ru)–π*(NCS) → π*(anci) π*(thi)
		497.8 (2.49)	0.0377	H−0 → L+2(0.39)	d_{xz}(Ru)–π*(NCS) → π*(anch)
				H−2 → L+1(0.34)	d_{yz}(Ru)–π*(NCS) → π*(anci) π*(thi)
				H−1 → L+1(0.32)	d_{xy}(Ru)–π*(NCS) → π*(anci) π*(thi)
				H−2 → L+0(0.31)	d_{yz}(Ru)–π*(NCS) → π*(anci) π*(thi)
		488.6 (2.54)	0.1695	H−2 → L+1(0.59)	d_{yz}(Ru)–π*(NCS) → π*(anci) π*(thi)
				H−1 → L+1(0.23)	d_{xy}(Ru)–π*(NCS) → π*(anci) π*(thi)
				H−2 → L+0(0.20)	d_{yz}(Ru)–π*(NCS) → π*(anci) π*(thi)
	4	434.5 (2.85)	0.0578	H−2 → L+2(0.52)	d_{yz}(Ru)–π*(NCS) → π*(anch)
				H−1 → L+2(0.40)	d_{xy}(Ru)–π*(NCS) → π*(anch)

in DMF, the 10–20 nm blue-shifts should be considered as solvent effect.

For **II** system, the absorption curve and character are nearly as the same as **I** system shown in Figure 5 and Supporting Information, Table S3. It could be concluded that the effect of expanding conjugated plane is not ideal for improving the absorption in visible range.

Absorption spectra of III and IV in ACN. The fitted Gaussian-type absorption curves are shown in Figures 6 and 7 for **III** and **IV** systems, Compared with **I** and **II**, the characters of transitions are very simple, all of which could be concluded as ML_1CT and L_3L_1CT at $\lambda > 400$ nm. From the absorption data in Table 4, it could be seen that the improvement of ancillary ligand is significant to absorptions in visible range especially the corresponding oscillator strengths are strengthened, and the absorption intensity has hardly relationship with degree of deprotonation in these system. For **III** system alone, ancillary ligands make more contribution to absorptions than anchoring ligands, even for **III** (**2H**–**0H**), only several transitions have no relation with them. Furthermore, the contribution of thiophene is very tremendous from 460 to 570 nm, which is different from benzene in **IV** system. Notably, the oscillator strengths in **III** system are generally stronger than others shown in Figures 4–7. For **III** (**1H**) and **III** (**0H**), there are also strong absorptions from 400 to 600 nm, which is different from the systems before. Briefly, it could be anticipated that all the dye molecules in **III** have great potential to be an efficient DSSCs.

The most obvious difference is about oscillator strength between **III** and **IV** systems. As the local energy of benzene is little higher than thiophene, only several delocalized orbitals have relationship to benzene group in **IV** (**2H**), and the effect of improvement for ancillary ligands is not as well as **III**. However, oscillator strengths of absorption are stronger than **I** and **II** systems on the basis of absorption transitions and the optical spectrum properties of **IV** is superior to **I** and **II**.

Finally, the tactics of connecting the conjugated group on the ancillary ligand can efficiently tunes energy levels distribution of LUMOs and bring about amply absorption spectrum, which is better for seeking higher photon to current conversion efficiency in DSSCs.

Emission spectra

In view of obtaining the convincing emissive energy, based on the excited-state structures optimized by the UB3LYP method, the emission spectra of complexes **III** from **2H** to **0H** in solution (ACN) are calculated by TDDFT approach at the B3LYP level. The corresponding emissions of **III** (**2H**–**0H**) are listed in Table 5, associated with the emissive energies and transition assignments.

Table 5. Phosphorescent emission of III (2H–0H) in ACN by TD-B3LYP (6–31G*).

III	Medium	Transition	Config (CI coeff)	E_{nm} (eV)	Assignment
2H	ACN	$^3A \rightarrow {}^1A$	H−0 → L+0 (0.69)	996.7 (1.24)	^{3}MLCT/^{3}LLCT
1H	ACN	$^3A \rightarrow {}^1A$	H−0 → L+0 (0.64)	800.4 (1.55)	^{3}MLCT/^{3}LLCT
0H	ACN	$^3A \rightarrow {}^1A$	H−0 → L+0 (0.63)	838.5 (1.48)	^{3}MLCT/^{3}LLCT

The calculated phosphorescences in ACN solution for **III** (**2H**–**0H**) are at 997, 800, and 838 nm, respectively. The phosphorescent emissions are assigned to originate from the ^{3}MLCT/^{3}LLCT excited state. We have presented in above discussions that the lowest energy absorptions calculated at 699, 636, and 599 nm for **III** (**2H**–**0H**), respectively, also arise from the MLCT/LLCT transition. As the lowest energy emissions and absorptions have the same symmetry and transition character for each complex, the phosphorescent emissions should be the reverse process of the lowest energy absorptions. The Stokes shifts between the lowest energy absorptions and emissions are 0.53 **III** (**2H**), 0.40 **III** (**1H**), and 0.59 eV **III** (**0H**). These small shifts are in agreement with the small change between ground- and excited-state structures, and the design-rationality of these complexes could be checked in emissions.

We expect that the experimental data will be available in academic community in the future, and the further credibility of the simulation calculation could be obtained.

Conclusions

Electronic structures and spectroscopic properties of **I**, **II**, **III**, and **IV** (**2H**–**0H**) were investigated theoretically. We predicted the absorption and emission spectra in solution using the TDDFT method with the solvent-effect PCM model. Taking into account the deprotonation effect, the following conclusions can be drawn.

The analysis of the electronic structures for **2H**–**0H** in four systems shows that the deprotonation effect leads to a sizable difference in the electronic structures. In the cases of both absorption and emission, the energy levels of occupied MOs and unoccupied MOs for **2H**–**0H** increase obviously along with the degree of deprotonation. For each step of deprotonation, the destabilization of the unoccupied orbitals is larger with respect to the occupied orbitals. Thus, the HOMO–LUMO gaps of absorptions and emissions increases from **2H** to **0H**. This tendency is harmful to absorptions, because the high energy gap leads electron transition difficultly.

On the contrary, it is shown that the choice of ancillary ligands is important for absorptions and assignment of energy levels. In visible range, the absorption could be intensified when the ancillary ligand is involved. Besides, the deprotonation can enhance more energy of orbitals on the anchoring ligand than that on the ancillary ligand. As the multiplicity of MOs on ancillary ligands is high, there are two similar energy orbitals localized on ancillary ligands for unoccupied MOs particularly in **I** and **III** systems. When the two orbitals become the lowest energy unoccupied MOs along with the increasing of degree of deprotonation, the absorption can be reinforced in high degree of deprotonation, and the more efficient DSSCs could be detected.

Overall, for the absorption improvement, there is a well tactics, that the thiophene is adopted to connected to ancillary ligands. This modification not only widens absorption range but also increases oscillator strengths. Finally, **III** system is optimal candidate of efficient dye molecules in DSSCs, whose absorbing intensity do not change sharply due to the two factors above, when the pH varies in certain range. Actually, this kind of dye molecules has never been found out before.

Keywords: dye-sensitized solar cell · density functional theory · derivatives of AR20 · energy levels · absorption spectrum · deprotonation

How to cite this article: J. Chen, J. Wang, F.-Q. Bai, Q.-J. Pan, H.-X. Zhang, *Int. J. Quantum Chem.* **2013**, *113*, 891–901. DOI: 10.1002/qua.24009

[1] B. O. Regan, M. Grätzel, *Nature* **1991**, *353,* 737.
[2] A. Hagfeldt, M. Grätzel, *Acc. Chem. Rev.* **2000**, *33,* 269.
[3] M. Grätzel, *Nature* **2001**, *414,* 338.
[4] K. Kalyanasundaram, M. Grätzel, *Coord. Chem. Rev.* **1998**, *177,* 347.
[5] K. Hara, T. Sato, R. Katoh, *J. Phys. Chem. B* **2003**, *107,* 597.
[6] T. Horiuchi, H. Miura, K. Sumioka, S. Uchida, *J. Am. Chem. Soc.* **2004**, *126,* 12218.
[7] A. Morandeira, G. Boschloo, A. Hagfeldt, L. Hammarstrolm, *J. Phys. Chem. B* **2005**, *109,* 19403.
[8] S. Ito, S. M. Zakeeruddin, R. Humphry-Baker, *Adv. Mater.* **2006**, *18,* 1202.
[9] D. Kuciauskas, M. S. Freund, H. B. Gray, J. R. Winkler, N. S. Lewis, *J. Phys. Chem. B* **2001**, *105,* 392.

[10] A. Islam, H. Sugihara, K. Hara, L. P. Singh, R. Katoh, M. Yanagida, Y. Takahashi, S. Murata, H. Arakawa, *Inorg. Chem.* **2001**, *40,* 5371.
[11] Q. Wang, W. M. Campbell, E. E. Bonfantani, K. W. Jolley, D. L. Officer, *J. Phys. Chem. B* **2005**, *109,* 15397.
[12] E. A. M. L. Geary, J. Yellowlees, L. A. Jack, I. D. H. Oswald, *Inorg. Chem.* **2005**, *44,* 242.
[13] M. K. Nazzruddin, A. Kay, I. Rodicio, R. Humphry-Baker, *J. Am. Chem. Soc.* **1993**, *115,* 6382.
[14] M. K. Nazeeruddin, S. M. Zakeeruddin, R. Humphry-Baker, M. Jirousek, P. Liska, *Inorg. Chem.* **1999**, *38,* 6298.
[15] M. K. Nazeeruddin, P. Pechy, T. Renouard, S. M. Zakeeruddin, *J. Am. Chem. Soc.* **2001**, *123,* 1613.
[16] N. O. Komatsuzaki, M. Yanagida, T. Funaki, K. Kasuga, K. Sayama, H. Sugihara, *Sol. Energy Mater. Sol. Cells* **2011**, *95,* 310.
[17] S. R. Jang, M. J. Choi, R. Vittal, K. J. Kim, *Sol. Energy Mater. Sol. Cells* **2007**, *91,* 1209.
[18] M. K. Nazeeruddin, F. De Angelis, S. Fantacci, A. Selloni, G. Viscardi, P. Liska, S. Ito, B. Taleru, M. Grätzel, *J. Am. Chem. Soc.* **2005**, *127,* 16835.
[19] (a) P. Wang, C. Klein, R. Humphry-Baker, S. M. Zakeeruddin, M. Grätzel, *J. Am. Chem. Soc.* **2005**, *127,* 808; (b) P. Wang, C. Klein, R. Humphry--Baker, S. M. Zakeeruddin, M. Grätzel, *Appl. Phys. Lett.* **2005**, *86,* 123508.
[20] F. F. Gao, Y. Wang, D. Shi, J. Zhang, M. Wang, X. Y. Jing, R. Humphry-Baker, P. Wang, S. M. Zakeeruddin, M. Grätzel, *J. Am. Chem. Soc.* **2008**, *130,* 10720.
[21] C. Y. Chen, J. G. Chen, S. J. Wu, J. -Y. Li, C. G. Wu, K. C. Ho, *Angew. Chem. Int. Ed.* **2008**, *47,* 7342.
[22] H. Kisserwan, T. H. Ghaddar, *Inorg. Chim. Acta* **2010**, *363,* 2409.
[23] D. Shi, N. Pootrakulchote, R. Li, J. Guo, Y. Wang, S. M. Zakeeruddin, M. Grätzel, P. Wang, *J. Phys. Chem. C* **2008**, *112,* 17046.
[24] A. Reynal, A. Forneli, E. Martinez-Ferrero, *J. Am. Chem. Soc.* **2008**, *130,* 13558.
[25] S. L. H. Higgins, T. A. White, B. S. J. Winkel, K. J. Brewer, *Inorg. Chem.* **2011**, *50,* 463.
[26] S. Ramachandra, K. C. Schuermann, F. Edafe, P. Belser, C. A. Nijhuis, W. F. Reus, G. M. Whitesides, L. De Cola, *Inorg. Chem.* **2011**, *50,* 1581.
[27] J. Bisquert, D. Cahen, G. Hodes, S. Ruehle, A. Zaban, *J. Phys. Chem. B* **2004**, *108,* 8106.
[28] M. K. Nazeeruddin, R. Humphry-Baker, P. Liska, M. Grätzel, *J. Phys. Chem. B* **2003**, *127,* 8981.
[29] W. M. Campbell, A. K. Burrell, D. L. Officer, K. W. Jolley, *Coord. Chem. Rev.* **2004**, *248,* 1363.
[30] R. Su, W. D. Xue, Y. Feng, J. H. Wang, D. Yi, *Acta Phys. Chim. Sin.* **2009**, *25,* 947.
[31] S. Ardo, G. J. Meyer, *Chem. Soc. Rev.* **2009**, *38,* 115.
[32] S. Kim, J. K. Lee, S. O. Kang, J. Ko, J. -H. Yum, S. Fantacci, F. De Angelis, D. Di Censo, M. K. Nazeeruddin, M. Grätzel, *J. Am. Chem. Soc.* **2006**, *128,* 16701.
[33] A. D. Becke, *Chem. Phys.* **1993**, *98,* 5648.
[34] (a) M. E. Casida, C. Jamorski, K. C. Casida, D. R. Salahub, *J. Chem. Phys.* **1998**, *108,* 4439; (b) R. E. Stratmann, G. E. Scuseria, *J. Chem. Phys.* **1998**, *109,* 8218; (c) N. N. Matsuzawa, A. Ishitani, *J. Phys. Chem. A* **2001**, *105,* 4953.
[35] (a) V. Barone, M. Cossi, *J. Phys. Chem. A* **1998**, *102,* 1995; (b) M. Cossi, N. Rega, G. Scalmani, V. Barone, *J. Comput. Chem.* **2003**, *24,* 669.
[36] M. Caricato, B. Mennucci, J. Tomasi, F. Ingrosso, R. Cammi, S. Corni, G. Scalmani, *J. Chem. Phys.* **2006**, *124,* 124520.
[37] B. Mennucci, C. Cappelli, C. A. Guido, R. Cammi, J. Tomasi, *J. Phys. Chem. A* **2009**, *113,* 3009.
[38] (a) R. Bauernschmitt, R. Ahlrichs, *Chem. Phys. Lett.* **1996**, *256,* 454; (b) A. Rosa, E. J. Baerends, S. J. Gisbergen, *J. Am. Chem. Soc.* **1999**, *121,* 10356.
[39] (a) W. R. Wadt, P. J. J. Hay, *Chem. Phys.* **1985**, *82,* 284; (b) P. J. Hay, W. R. Wadt, *J. Chem. Phys.* **1985**, *82,* 299.
[40] Gaussian 09, Revision A.1, M. J. Frisch, G. W. Trucks, H. B. Schlegel, G. E. Scuseria, M. A. Robb, J. R. Cheeseman, G. Scalmani, V. Barone, B. Mennucci, G. A. Petersson, H. Nakatsuji, M. Caricato, X. Li, H. P. Hratchian, A. F. Izmaylov, J. Bloino, G. Zheng, J. L. Sonnenberg, M. Hada, M. Ehara, K. Toyota, R. Fukuda, J. Hasegawa, M. Ishida, T. Nakajima, Y. Honda, O. Kitao, H. Nakai, T. Vreven, J. A. Montgomery, Jr., J. E. Peralta, F. Ogliaro, M. Bearpark, J. J. Heyd, E. Brothers, K. N. Kudin, V. N. Staroverov, R. Kobayashi, J. Normand, K. Raghavachari, A. Rendell, J. C. Burant, S. S. Iyengar, J. Tomasi, M. Cossi, N. Rega, J. M. Millam, M. Klene, J. E. Knox, J. B. Cross, V. Bakken, C. Adamo, J. Jaramillo, R. Gomperts, R. E. Stratmann, O. Yazyev, A. J. Austin, R. Cammi, C. Pomelli, J. W. Ochterski, R. L. Martin, K. Morokuma, V. G. Zakrzewski, G. A. Voth, P. Salvador, J. J. Dannenberg, S. Dapprich, A. D. Daniels, Ö. Farkas, J. B. Foresman, J. V. Ortiz, J. Cioslowski, D. J. Fox, Gaussian Inc., Wallingford CT, **2009**.
[41] J. Chatt, L. A. Duncanson, *J. Chem. Soc.* **1953**, 2939.
[42] P. Boulet, H. Chermette, C. Daul, F. Gilardoni, F. Rogemond, J. Weber, G. Zuber, *J. Phys. Chem. A* **2001**, *105,* 885.
[43] J. E. Monat, J. H. Rodriguez, J. K. McCusker, *J. Phys. Chem. A* **2002**, *106,* 7399.
[44] S. Fantacci, F. De Angelis, A. Selloni, *J. Am. Chem. Soc.* **2003**, *125,* 4381.
[45] C. Barolo, M. K. Nazeeruddin, S. Fantacci, D. D. Censo, P. Comte, P. Liska, G. Viscard, P. Quagliotto, F. De Angelis, S. Ito, M. Grätzel, *Inorg. Chem.* **2006**, *45,* 4642.
[46] F. D. Angelis, S. Fantacci, A. Selloni, *Chem. Phys. Lett.* **2004**, *389,* 204.

Received: 16 November 2011
Revised: 16 November 2011
Accepted: 17 November 2011
Published online on 13 February 2012